

New Methodologies for True Orthophoto Generation

Ayman F. Habib, Eui-Myoung Kim, and Chang-Jae Kim

Abstract

Orthophoto production aims at the elimination of sensor tilt and terrain relief effects from captured perspective imagery. Uniform scale and the absence of relief displacement in orthophotos make them an important component of GIS databases, where the user can directly determine geographic locations, measure distances, compute areas, and derive other useful information about the area in question. Differential rectification has been traditionally used for orthophoto generation. For large scale imagery over urban areas, differential rectification produces serious artifacts in the form of double mapped areas at object space locations with sudden relief variations, e.g., in the vicinity of buildings. Such artifacts are removed through true orthophoto generation methodologies which are based on the identification of occluded portions of the object space in the involved imagery. Existing methodologies suffer from several problems such as their sensitivity to the sampling interval of the digital surface model (DSM) as it relates to the ground sampling distance (GSD) of the imaging sensor. Moreover, current methodologies rely on the availability of a digital building model (DBM), which requires an additional and expensive pre-processing. This paper presents new methodologies for true orthophoto generation while circumventing the problems associated with existing techniques. The feasibility and performance of the suggested techniques are verified through experimental results with simulated and real data.

Introduction

Remote sensing imagery are usually acquired through perspective projection, where reflected light rays from the object space pass through the perspective center of the imaging sensor. Such a projection results in scale variation and relief displacement in the acquired imagery. Orthophoto generation aims at eliminating relief displacement from perspective imagery. As a result, orthophotos are characterized by having a uniform scale and showing objects in their true geographical locations. In other words, orthophotos have the same characteristics of a map. Therefore, the user can position objects, measure distances, compute areas, quantify changes, and derive other useful information from available orthophotos. Such uses make orthophotos an

important component of GIS databases. The production of orthophotos requires the availability of a digital image, a digital surface model (DSM), as well as the internal and external characteristics of the imaging sensor (Kraus, 1993). With the increased adoption of digital cameras, lidar systems, and GPS/INS geo-referencing units, the mapping community has easy access to all the essential components for orthophoto production.

Orthophotos are generated through a rectification process, which might be direct or indirect (Konecny, 1979; Novak, 1992). Direct rectification utilizes the internal and external characteristics of the imaging sensor to directly project the image contents onto the DSM cells. Direct orthophoto generation is carried out through an iterative process. The mechanics of the direct orthophoto generation might leave some of the cells in the DSM with unassigned gray values. Therefore, empty cells have to be interpolated from neighboring ones. In contrast to the direct rectification, indirect orthophoto generation starts by projecting the DSM cell vertices onto the image plane using the internal and external sensor characteristics. The gray value at the projected image location is interpolated using the ones at neighboring cells/pixels. Finally, the interpolated gray value is assigned to the corresponding DSM vertex. Differential rectification is the commonly used term to denote indirect rectification of perspective imagery (Konecny, 1979; Novak, 1992). The conceptual procedure for ortho-rectification is illustrated in Figure 1.

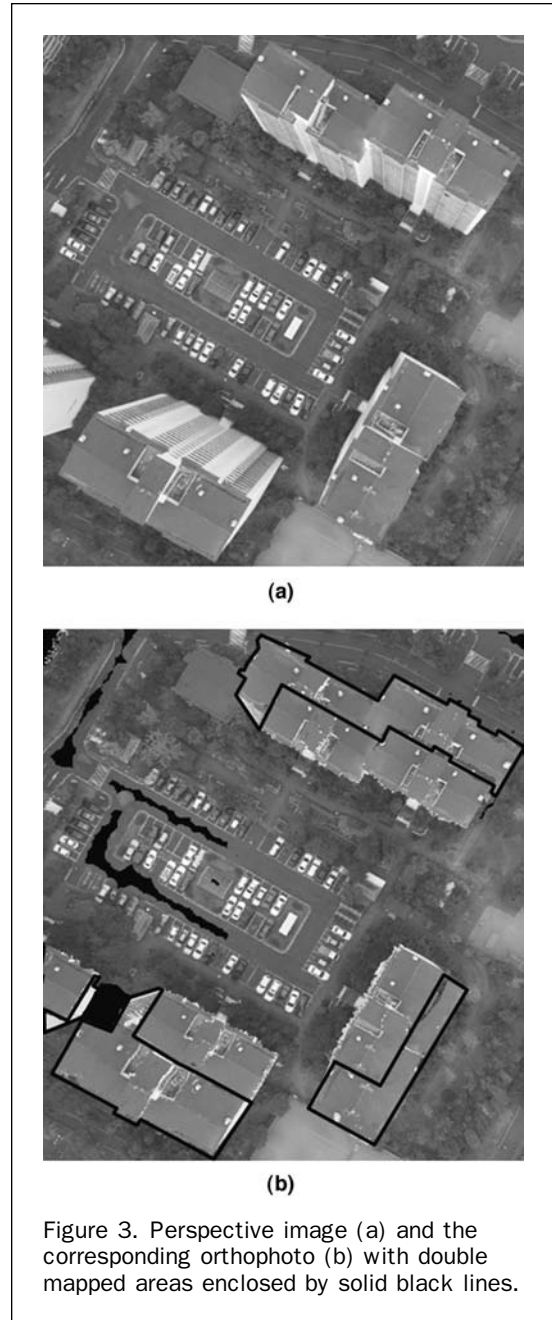
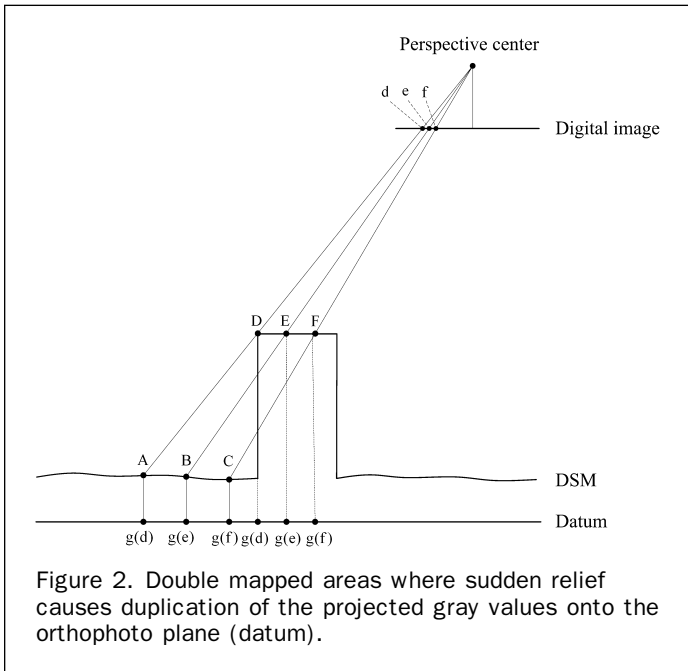
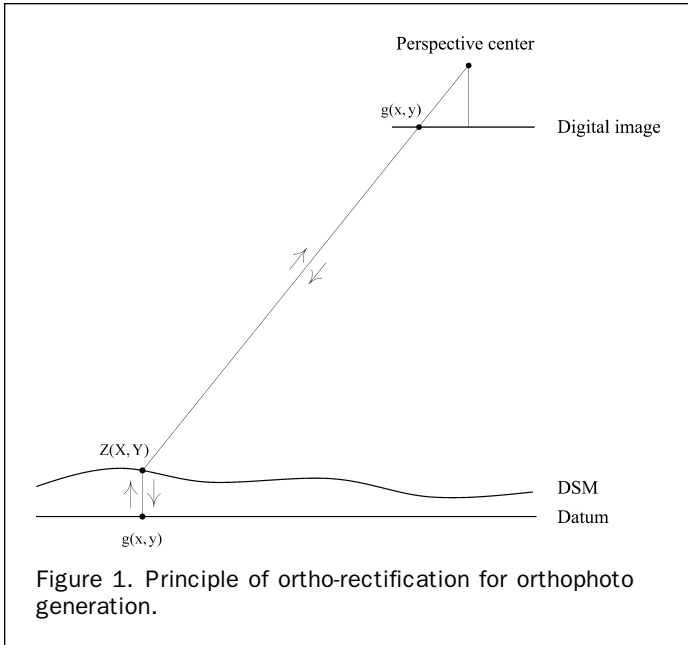
When dealing with large scale imagery over urban areas, differential rectification produces a significant artifact, which is the double mapped areas at the vicinity of abrupt surface changes (Skarlatos, 1999). Figure 2 is a schematic diagram illustrating the double mapping problem. In Figure 2, points D , E , and F along the DSM are projected onto the image plane at the locations d , e , and f , respectively. The interpolated gray values $g(d)$, $g(e)$, and $g(f)$ are assigned to the corresponding DSM cells. On the other hand, due to the relief displacement caused by the vertical structure, the gray values $g(d)$, $g(e)$, and $g(f)$ will be also assigned to the DSM at the locations A , B , and C , respectively. Therefore, these gray values will be incorrectly duplicated in the orthophoto plane (datum) causing double mapping of the same area. A real example of the double mapping problem is illustrated in Figure 3, where the perspective image and the generated orthophoto are shown. As it can be seen in Figure 3a, the vertical structures have significant relief displacements that cause

Ayman F. Habib and Chang-Jae Kim are with the Department of Geomatics Engineering, University of Calgary, Calgary, Alberta, Canada T2N 1N4 (habib@geomatics.ucalgary.ca; cjkim@ucalgary.ca).

Eui-Myoung Kim is with the KSIC (Korea geoSpatial Information and Communication Corporation), Seoul, Korea (kemyoung@ksic.net).

Photogrammetric Engineering & Remote Sensing
Vol. 73, No. 1, January 2007, pp. 025–036.

0099-1112/07/7301-0025/\$3.00/0
© 2007 American Society for Photogrammetry
and Remote Sensing



considerable occlusions in the object space. The generated orthophoto in Figure 3b shows that the relief effects along the building facades have been removed. However, double mapped areas, which are enclosed by solid black lines, occupy occluded portions of the object space. Double mapped areas constitute a severe degradation and are a major obstacle to the interpretability of the generated orthophoto. Therefore, true orthophoto generation methodologies focus on the elimination of the double mapped areas. The basic principle of these methodologies is the identification of occluded areas, which are caused by relief displacements associated with vertical structures in the object space.

True orthophoto generation is mainly concerned with visibility analysis, which has been studied in computer graphics, computer vision, photogrammetry, remote sensing, and telecommunications. The classical visibility algorithms were developed in the early days of computer graphics: late

sixties and early seventies (Sutherland *et al.*, 1974). Amhar *et al.* (1996) proposed a methodology, which is based on photogrammetric principles, for making true orthophotos using digital terrain models (DTM) and digital building models (DBM). In this methodology, two orthophotos, one corresponding to the terrain while the other corresponds to the buildings, are independently generated. The DBM is first used to mask portions of the input image that are covered by man-made structures. The masked image is then used in conjunction with the DTM to generate the terrain orthophoto. In the mean time, the DBM together with the original image is used to generate the building orthophoto. The final true orthophoto is created by combining the terrain and building orthophotos. Therefore, the proposed methodology by Amhar *et al.* (1996) does not explicitly detect occluded areas. However, occlusions are implicitly considered by utilizing the masked image for the generation of the terrain orthophoto.

Kuzmin *et al.* (2004) proposed a polygon-based approach for the detection of obscured areas for true orthophoto generation. In this method, conventional differential rectification is first applied. Afterwards, hidden areas are detected by using polygonal surfaces, which are generated from a DBM. Other than the proposed methodology by Kuzmin *et al.*, the majority of existing true orthophoto generation techniques is based on the Z-buffer algorithm (Catmull, 1974; Amhar *et al.*, 1998; Rau *et al.*, 2000; Rau *et al.*, 2002; Sheng *et al.*, 2003; Zhou, 2005). As it can be seen in Figure 2, double mapped areas arise from the fact that two object space points (e.g., *A* and *D*, *B* and *E*, or *C* and *F*) are competing for the same image location (e.g., *d*, *e*, or *f*, respectively). The Z-buffer method resolves the ambiguity of which object point should be assigned to the image location by considering the distances between the perspective center and the object points in question. Among the competing object points, the closest point to the perspective center is considered visible while the other points are judged to be invisible in that image.

A common prerequisite for the above methodologies for true orthophoto generation is the need for a DBM. Moreover, the Z-buffer methodology has several limitations such as its sensitivity to the sampling interval of the DSM as it relates to the ground sampling distance (GSD) of the imaging sensor and the need for introducing artificial points (pseudo groundels) along building facades (Rau *et al.*, 2000; Rau *et al.*, 2002; Sheng *et al.*, 2003). In this paper, two new methodologies are proposed for true orthophoto generation while circumventing the limitations and expensive requirements of existing methodologies. The new methodologies do not require a DBM and are based on investigating the off-nadir angles of the DSM cells along radial directions from the object space nadir point. The following section briefly describes the Z-buffer methodology together with its limitations and drawbacks. This discussion will be followed by an explanation of the proposed techniques. Afterwards, experimental results with simulated and real data are presented to verify the feasibility and the performance of the suggested algorithms. Finally, conclusions and recommendations for future work are summarized.

Z-buffer Method

As it was mentioned earlier, the Z-buffer methodology for true orthophoto generation identifies occluded areas by resolving the ambiguity arising from having more than one object point competing for the same image pixel (Figure 2). As it was proposed by Amhar *et al.* (1998), the implementation of the Z-buffer starts by establishing three 2D arrays with the same dimensions of the input image, which will be referred to here forth as the Z-buffer arrays, and a visibility map with the same dimensions of the input DSM (Figure 4). Two out of the three Z-buffer arrays are used to record the *X* and *Y* coordinates of the DSM cell that is projected onto the corresponding image pixel. The third array stores the distances between the perspective center and the respective DSM cells. The visibility map, on the other hand, indicates whether the corresponding DSM cell is visible in the involved image or not.

To illustrate the conceptual basis of the Z-buffer methodology, one can start by considering the DSM cell *A* in Figure 4. After being projected onto the image plane, the corresponding pixels in the Z-buffer arrays are assigned the coordinates X_A and Y_A as well as the distance between the perspective center and the object point *A*, d_A . In the mean time, the corresponding cell in the visibility map is initialized to indicate a visible DSM cell. Such a process is repeated while considering other cells within the DSM. When dealing

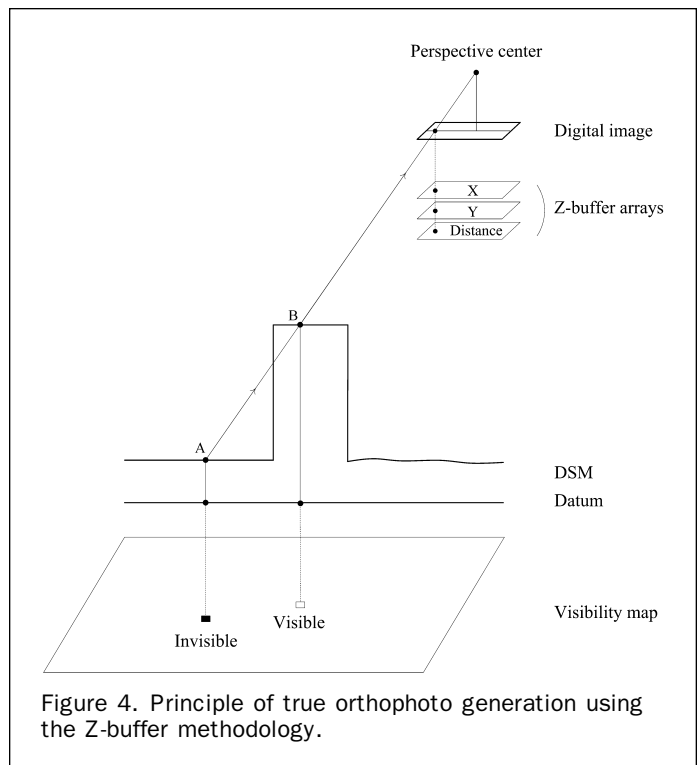


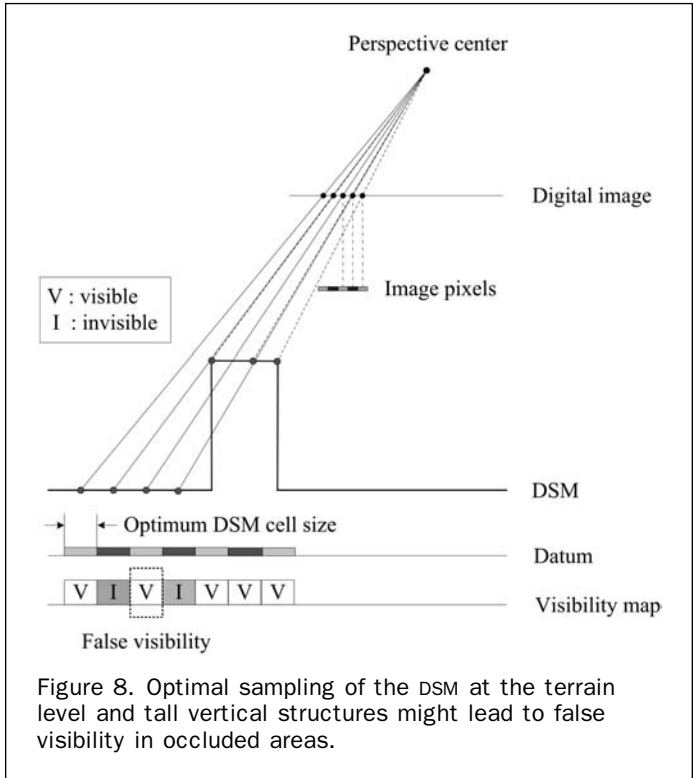
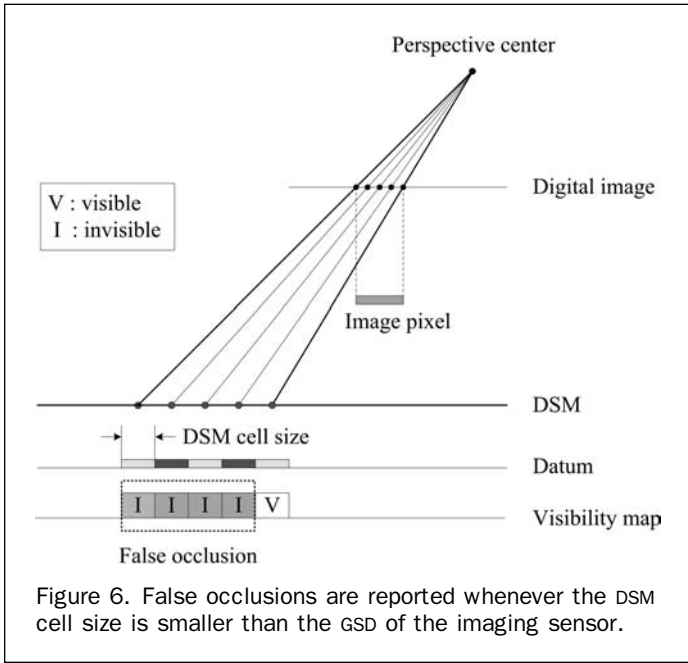
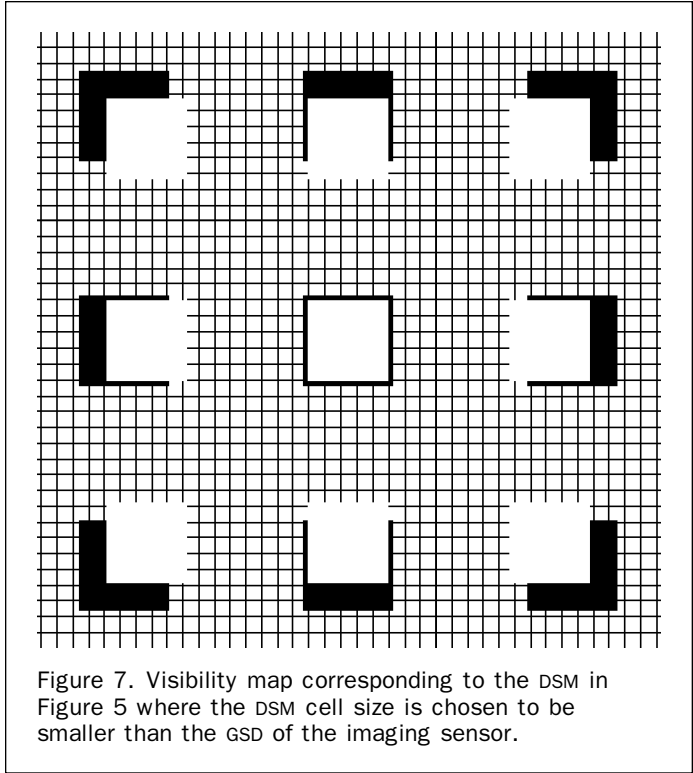
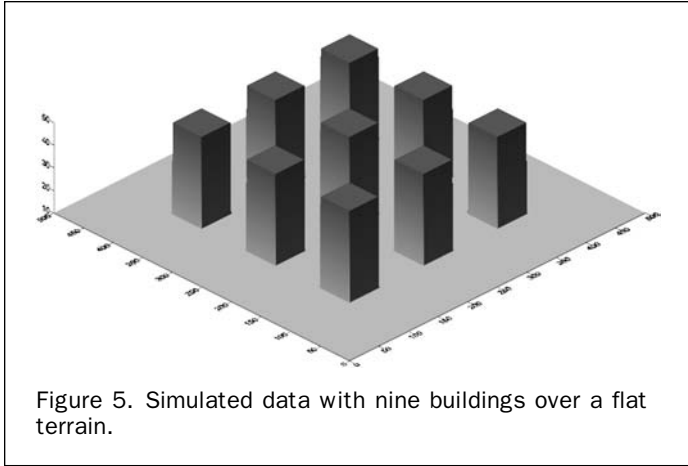
Figure 4. Principle of true orthophoto generation using the Z-buffer methodology.

with the DSM cell *B*, the algorithm determines that the corresponding image pixel has already been linked to the DSM cell *A*. To resolve which of the two DSM cells should be assigned to that image pixel, the distances from the perspective center to *A* and *B* (d_A and d_B , respectively) are computed and compared. Since d_A is greater than d_B , the DSM cell *B* is declared visible while *A* is deemed invisible. Therefore, the Z-buffer arrays are updated where X_A , Y_A , and d_A are replaced with X_B , Y_B , and d_B , respectively. In addition, the visibility map is modified to indicate that the DSM cell *A* is invisible, while *B* is visible. After considering all the cells within the DSM, the Z-buffer arrays are used to transfer the gray values from the input image to the corresponding locations in the orthophoto plane. In the mean time, the visibility map can be used to indicate occluded areas in the object space due to relief displacement effects.

The next subsections will briefly discuss the drawbacks of the Z-buffer methodology as well as possible solutions to mitigate the effects of these problems. To illustrate the manifestations of these drawbacks, a synthetic DSM consisting of nine buildings, 50 m high, over a flat terrain is generated (Figure 5). The perspective center of the simulated image over the DSM is located above the centroid of the central building. The performance of the Z-buffer methodology will be evaluated through the quality of detected occlusions.

DSM Cell Size Relative to the GSD of the Imaging Sensor

Detected occlusions by the Z-buffer methodology depend on the relative relationship between the DSM cell size and the GSD of the imaging sensor. If the DSM cell size is less than the GSD of the imaging sensor, false occlusions in flat areas will be reported. Figure 6 illustrates such an instance, where several DSM cells not occluding each other are projected onto the same image pixel. As a result, the DSM cell, which is closest to the projection center, will be deemed visible, while the others are incorrectly considered to be occluded. Another illustration of such a phenomenon



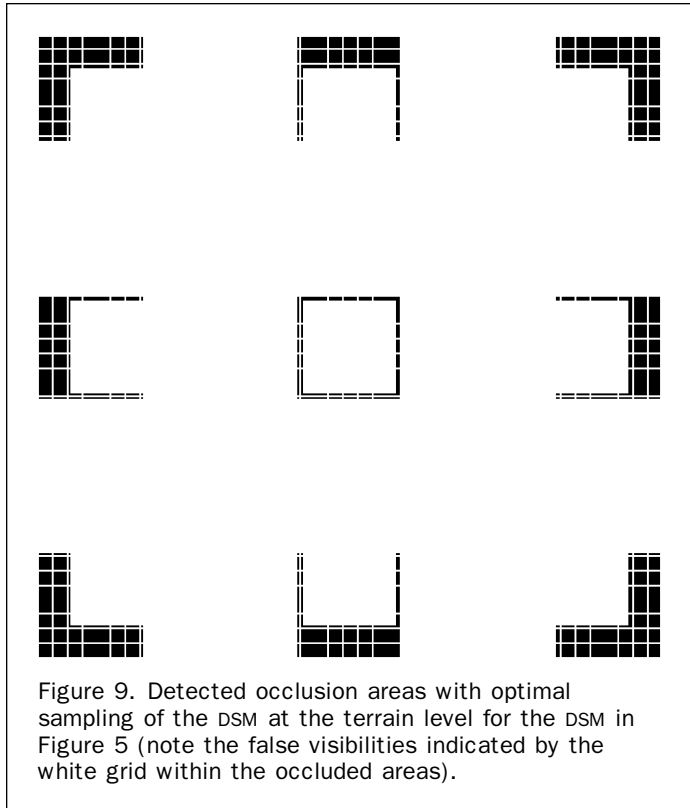
is depicted in Figure 7, which shows the visibility map associated with the DSM in Figure 5. Black portions in this map indicate occluded areas. As it can be seen in this figure, the over sampling of the DSM would lead to false occlusions, as represented by the black grid in between the buildings.

To avoid these false occlusions, the DSM cell size should be made equivalent to the GSD of the imaging sensor. However, the GSD is uniquely defined if and only if one is dealing with a vertical image over flat and horizontal terrain. Therefore, choosing the DSM cell size to be equivalent to the nominal GSD will not guarantee the absence of incorrectly detected occlusions. A related problem to the DSM cell size is shown in Figure 8. In this case, the DSM cell size is chosen to be equivalent to the GSD at the terrain surface. However, such a choice will lead to having non-compatible resolutions at the building roofs. As a result, false visibility will be reported in the occluded areas by vertical structures. Further illustration of this problem is depicted in Figure 9, where false visibility, as represented by a white grid, is detected within the occlusions associated with the vertical structures in Figure 5. The false visibility problem will escalate as the

height of the vertical structures becomes significant in relation to the flying height of the imaging sensor.

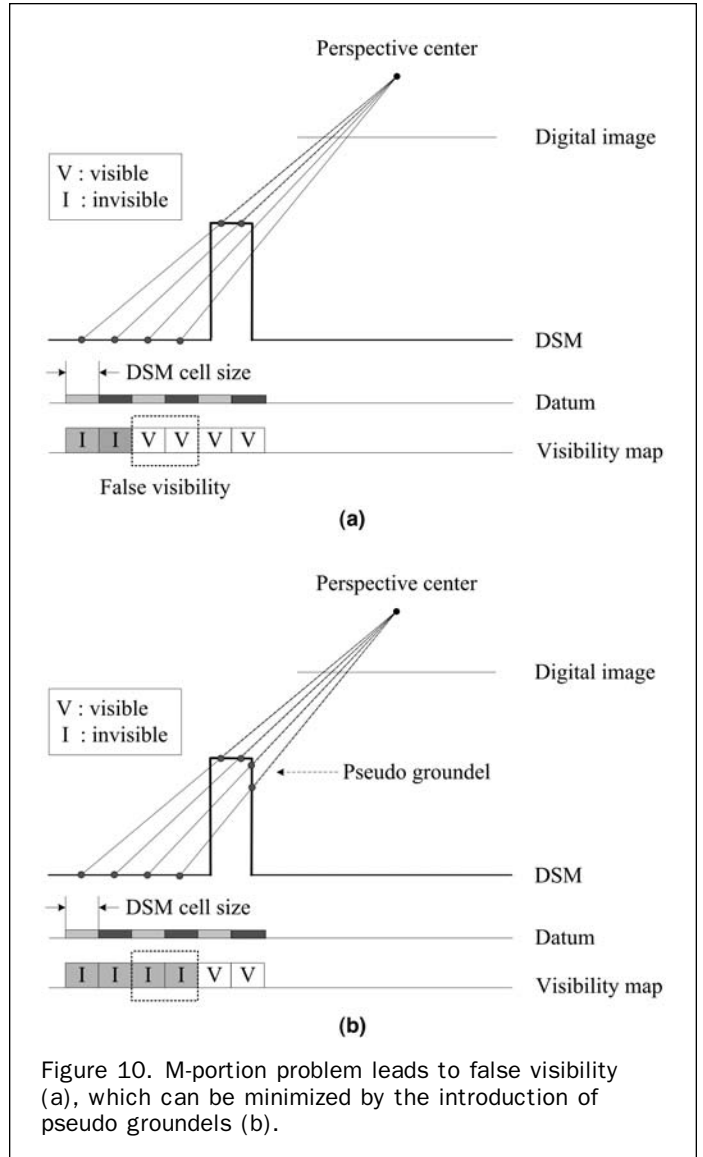
Narrow Vertical Structures

Another significant defect of the Z-buffer methodology is the false visibility associated with narrow vertical structures. This problem is commonly known in the photogrammetric literature



as the M-portion problem (Rau *et al.*, 2000 and 2002). The M-portion problem is shown in Figure 10. In this case, some of the pixels in the occluded area do not have any competition from points on the building roof (as represented by Figure 10). In such a case, terrain points in the occluded area will be incorrectly deemed visible as seen in Figure 10a. To minimize this problem, additional pseudo groundels are introduced along the facades of vertical structures (Figure 10b). In such a case, a digital building model (DBM) should be available. False visibility caused by the M-portion problem as well as improved occlusion detection after the introduction of pseudo groundels for one of the buildings in Figure 5 are shown in Figures 11a and 11b, respectively. It should be noted that the pseudo groundels also reduce the false visibilities that have been reported in the previous section, which have been shown in Figure 9.

In summary, to minimize the problems associated with the Z-buffer methodology, it should be preceded by interpolating the DSM to a resolution that is equivalent to the nominal GSD of the imaging sensor. Moreover, a DBM should be available to allow for the introduction of pseudo groundels along the facades of vertical structures. However, these precautions would not guarantee the absence of false occlusions or visibilities in the resulting true orthophoto. Therefore, generated orthophotos from the Z-buffer methodology are post-processed using a majority filter to eliminate sporadic false visibilities or occlusions. The following section introduces two new methodologies, which have been developed to avoid the problems of the Z-buffer technique. The developed methodologies detect occlusions by checking the off-nadir angle of the line of sight connecting the perspective center with the object point in question. Therefore, the proposed methodologies will be categorized as angle-based true orthophoto generation methodologies in contrast to the distance-based strategy implemented within the Z-buffer methodology.



Angle-based True Orthophoto Generation

In an orthogonal projection, points are vertically dropped onto the datum. Therefore, when considering a vertical structure, its top and bottom are projected onto the same location without any relief displacement. However, in a perspective projection, the top and bottom of that structure will be projected as two points which are spatially separated by the relief displacement. This displacement is expected to take place along a radial direction emanating from the image space nadir point (Mikhail, 2001). The radial extent of the relief displacement is the source of occlusions/invisibilities in perspective imagery. The presence of occlusions can be discerned by sequentially checking the off-nadir angles to the lines of sight connecting the perspective center to the DSM points along a radial direction starting from the object space nadir point. In the remainder of this paper, the off-nadir angle to the line of sight will be denoted the α angle (Figure 12).

Since there is no relief displacement associated with the object space nadir point, one can assure that this point will be always visible in the acquired image. As one moves away from the object space nadir point, it is expected that the α angle will increase continuously. As long as there is an increase in the α angle as one moves away from the nadir

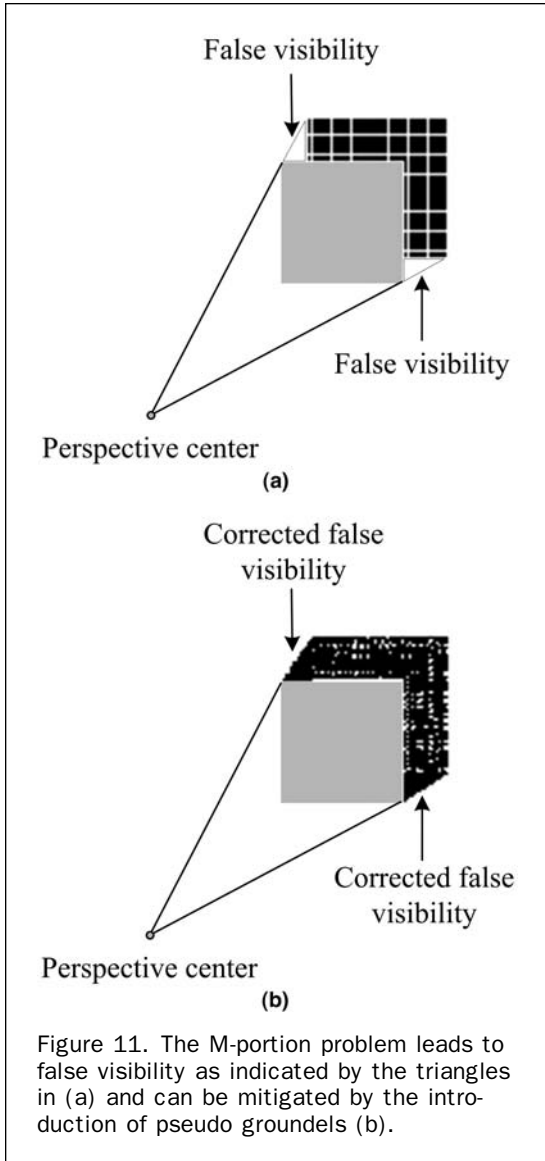


Figure 11. The M-portion problem leads to false visibility as indicated by the triangles in (a) and can be mitigated by the introduction of pseudo groundels (b).

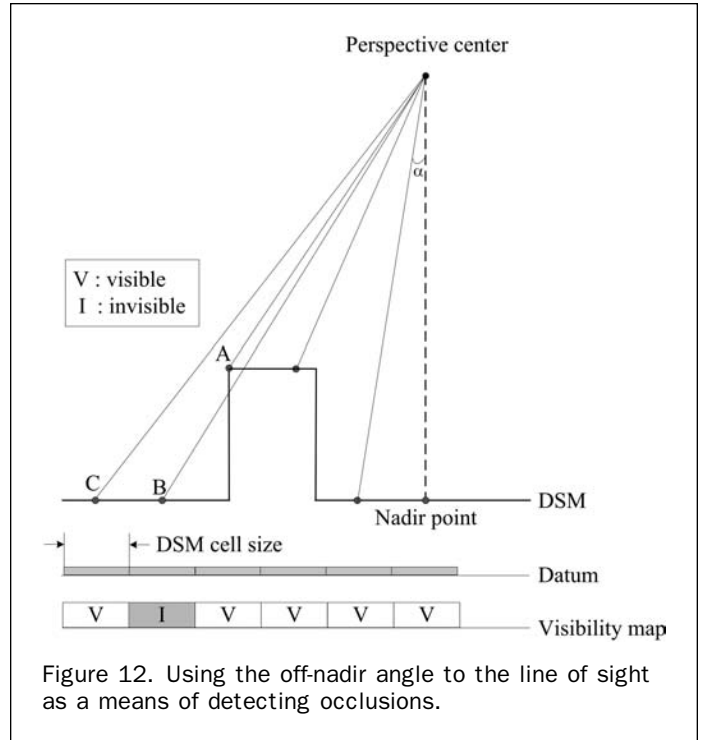


Figure 12. Using the off-nadir angle to the line of sight as a means of detecting occlusions.

introduced for occlusion detection and true orthophoto generation. The difference between these methods resides in the sequence of checking the α angle. As the names might suggest, the radial sweep detects occlusions while sweeping the DSM one radial direction at a time. On the other hand, the spiral sweep detects occlusions while sweeping the DSM in a spiral mode starting from the object space nadir point.

Adaptive Radial Sweep Method

As it was mentioned before, checking the α angle along radial directions from the nadir point can be used to identify occluded cells in DSM. The radial sweep method considers individual cells in the DSM by scanning through the radial directions from the object space nadir point. For example, one can start by considering the radial direction with zero azimuth (i.e., $\theta_0 = 0$ as in Figure 13). After classifying the DSM cells along that direction, one would move to the next radial direction by incrementing the azimuth with a given

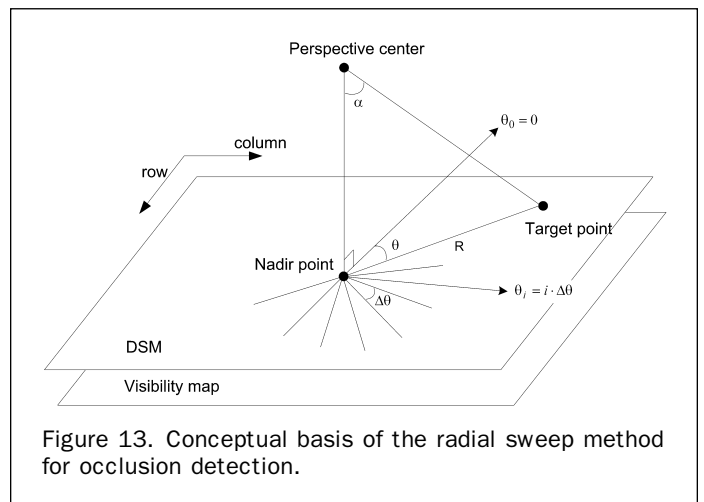


Figure 13. Conceptual basis of the radial sweep method for occlusion detection.

point while considering DSM cells along the radial direction, these cells will be visible in that image. On the other hand, occlusions will take place whenever there is an apparent decrease in the α angle while proceeding away from the nadir point. This occlusion will persist until the α angle exceeds the angle associated with the last visible point. Figure 12 illustrates the mechanics of using the off-nadir angle to the line of sight in detecting occluded areas by considering a vertical profile through the perspective center. As it can be seen in this figure, moving away from the nadir point will be accompanied by an increase in the α angle until one reaches the object point A; thus indicating no occlusion. However, when considering the object point B, one would notice that α_B is smaller than α_A , which indicates that point B is occluded by A. For the object point C, it is obvious that α_C is greater than α_A , which indicates that C is visible.

In summary, checking the α angle along a radial direction while moving away from the nadir point can be used for occlusion detection. The performance of such a methodology does not depend on the relative relationship between the DSM cell size and the GSD of the imaging sensor. Moreover, there is no need for having a DBM of the area in question. In this paper, two angle-based methodologies, which will be denoted as the adaptive radial sweep and spiral sweep, are

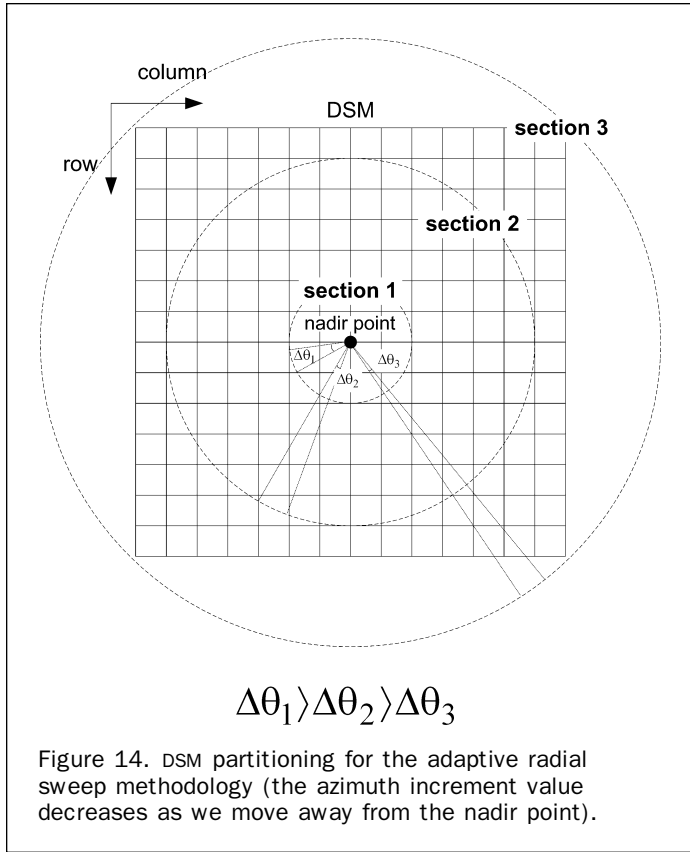


Figure 14. DSM partitioning for the adaptive radial sweep methodology (the azimuth increment value decreases as we move away from the nadir point).

value $\Delta\theta$. This process is repeated until the whole range of azimuth values is considered. Detected occlusions along the radial directions can be stored in a visibility map with the same dimensions as the DSM. This map is initially set by switching off all the cells to indicate an occlusion. Throughout the radial sweep search, non-occluded DSM cells will be switched on at the corresponding visibility map locations. Finally, the gray values at visible DSM cells are imported from the original image using the traditional differential rectification. In this way, occluded areas will be left blank, thus producing a true orthophoto.

A critical decision in the implementation of the radial sweep method is the choice of the azimuth increment value ($\Delta\theta$). A small value will be time consuming and inefficient since the DSM cells close to the nadir point will be repeatedly revisited. On the other hand, coarse selection of the

azimuth increment value will lead to non-visited DSM cells at the boundaries. To avoid this problem, an adaptive radial sweep is proposed, where the azimuth increment value is decreased gradually while moving away from the nadir point (Figures 14 and 15).

The implementation of the adaptive radial sweep for occlusion detection and true orthophoto generation can proceed according to the following steps (a conceptual procedural flow can be seen in Figure 16):

1. The DSM is divided into concentric rings centered at the object space nadir point (Figure 14).
2. Using the introduced sections in Step 1, one can define an R to θ array as shown in Figure 15, where R indicates the radial distance from the nadir point and θ is the corresponding azimuth for a given DSM cell. The R to θ array will be used to store the α angle associated with the DSM cells. The pixel size in the R-direction can be chosen to be equivalent to the DSM pixel size. The R-direction of the array is divided into sections that correspond to these identified in the previous step. Since various sections use different azimuth increment values, the number of rows in that array increases as the radial distance increases. More specifically, the azimuth increment value should vary for each section to assure that the majority of the DSM cells are visited without excessive repetition or gaps.
3. Define a visibility map with the same dimensions of the DSM grid. All the cells in the visibility map are switched off to indicate an occlusion. Also, define two arrays with the same dimensions of the R to θ array. These arrays will be used to store the X and Y coordinates of the corresponding cells in the DSM.
4. For each of the cells in the DSM, compute the corresponding R, θ , and α values. One should note that the R and θ values might not correspond to an integer location in the R to θ array. Therefore, the α angle is stored in the closest R to θ array element. In the mean time, the corresponding X and Y coordinates are stored in the respective X and Y arrays.
5. After populating the R to θ , X, and Y arrays, one can proceed by checking the α angle in the R to θ array for a given azimuth value. Visible locations along this direction should be updated in the visibility map using the corresponding coordinates in the X and Y arrays.
6. Finally, the gray values at visible DSM cells are imported from the original image using the traditional differential rectification procedure. In this way, occluded areas will be left blank, thus producing a true orthophoto.

One should note that the number of sections and the respective azimuth increment values will affect the efficiency of the adaptive radial sweep method and influence the storage requirements of this approach. To alleviate these requirements, the spiral sweep method has been developed,

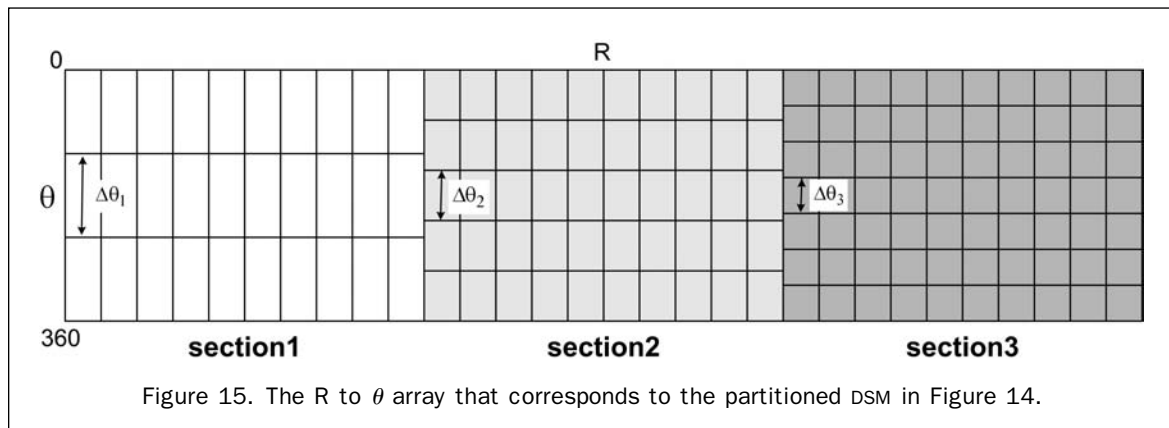


Figure 15. The R to θ array that corresponds to the partitioned DSM in Figure 14.

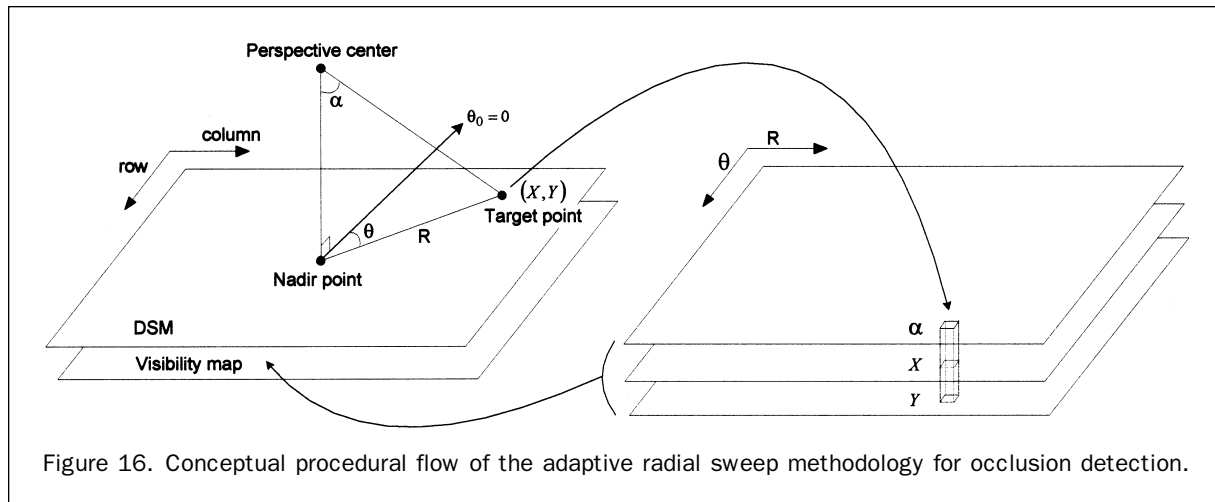


Figure 16. Conceptual procedural flow of the adaptive radial sweep methodology for occlusion detection.

where the DSM cells are swept in a spiral mode starting from the nadir point.

Spiral Sweep Method

Similar to the adaptive radial sweep algorithm, the spiral sweep method is an angle-based approach. However, the spiral sweep method scans the DSM cells starting from the nadir point in a spiral mode while directly checking the α angles along the radial directions without the need for DSM partitioning or additional arrays. The implementation of the spiral sweep requires a visibility map and an α array with the same dimensions of the DSM grid. Initially, all the cells in the visibility map are switched off to indicate an occlusion. The process starts by populating the α array by computing the off-nadir angle to the line of sight between the perspective center and the DSM cell in question. Afterwards, the α array is swept in a spiral mode as shown in Figure 17. For each cell in the α array, the α angle is compared to

the angle associated with the last visible point along the same radial direction from the nadir point. If the α angle of the cell in question is larger than the α angle of the last visible cell along the same radial direction, this cell will be considered visible and the corresponding cell in the visibility map is switched on. Finally, visible cells in the DSM are used to import the gray values from the input image according to the differential rectification procedure.

Experimental Results

To verify the performance of the developed methodologies, several experiments using simulated and real data were conducted. To compare the performance of the angle-based with existing distance-based approaches for true orthophoto generation, the Z-buffer methodology was also implemented. The results from simulated and real datasets are reported in the next two subsections.

Simulated Data

The simulated DSM in Figure 5 has been used for occlusion detection through the implementation of the adaptive radial sweep and spiral sweep methodologies. It should be noted that the results from the implementation of the Z-buffer methodology has been reported earlier in this paper. Detected occlusions from the adaptive radial sweep and spiral sweep methodologies are shown in Figures 18a and 18b, respectively. The dotted circles in Figure 18a indicate the number of the utilized sections within the adaptive radial sweep methodology. A closer look at Figure 18 reveals that the detected occlusions from the developed methodologies are almost identical except for very small differences at the occlusion boundaries. These differences are the result of number rounding of the involved values to the nearest integer. Comparing the detected occlusions with those resulting from the Z-buffer technique, one can see improved results without false visibilities and/or occlusions. In addition, the implementation of the new methodologies does not require any pre-processing to adjust the DSM cell size or having a DBM for the introduction of pseudo groundels along building facades.

Real Data

For further verification of the developed methodologies, additional experiments using real data have been conducted. The real data is comprised of twenty-three digital images, which were captured by a five megapixel Canon EOS-1-D digital camera and a lidar surface model over the City of

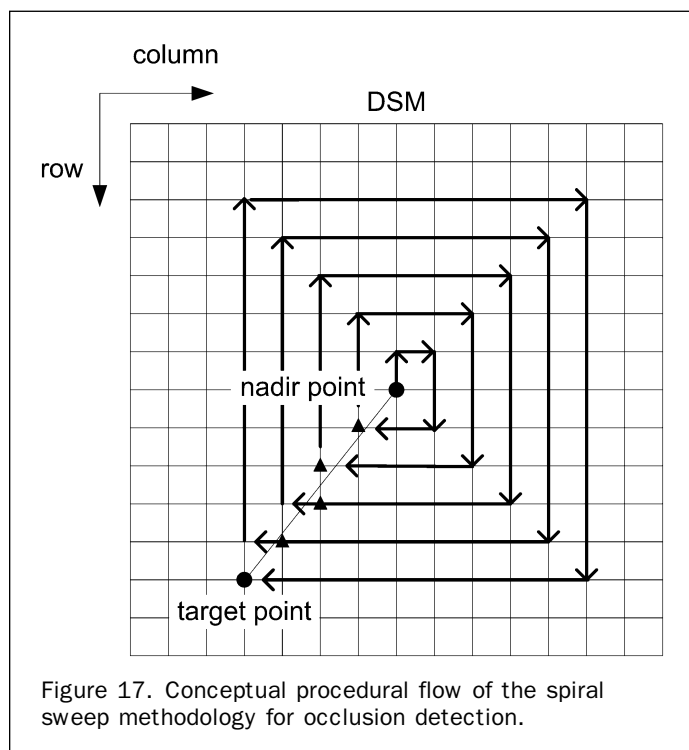


Figure 17. Conceptual procedural flow of the spiral sweep methodology for occlusion detection.

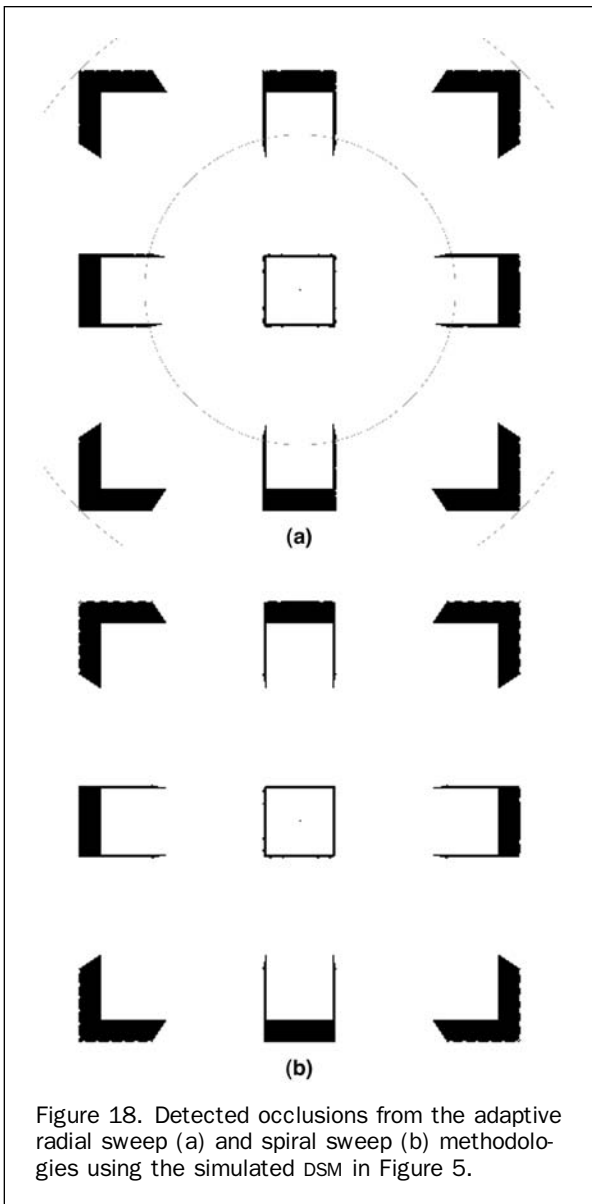


Figure 18. Detected occlusions from the adaptive radial sweep (a) and spiral sweep (b) methodologies using the simulated DSM in Figure 5.

Ilsan, South Korea. The exterior orientation parameters of the imaging sensor and the interior orientation parameters of the implemented camera are also available. Figure 3a and Figure 19 illustrate samples of the digital imagery and the DSM over the area of interest, respectively. As it can be seen in the image in Figure 3a, significant relief displacement and occlusions are present.

The generated true orthophotos from the adaptive radial sweep, spiral sweep, and Z-buffer methodologies are shown in Figures 20, 21, and 22, respectively. Black portions in these figures indicate occluded areas due to relief displacements at the buildings' locations. The figures also include a closer look at the vicinity of one building. Comparing Figures 20 and 21, one can see that the generated true orthophotos from the adaptive radial sweep and the spiral sweep methodologies are almost identical. In spite of the fact that the DSM cell size has been adjusted to be compatible with the GSD of the digital image as well as numerous pseudo groundels have been introduced along the building facades, the Z-buffer methodology is still showing false visibilities and occlusions (compare Figures 20, 21, and 22).

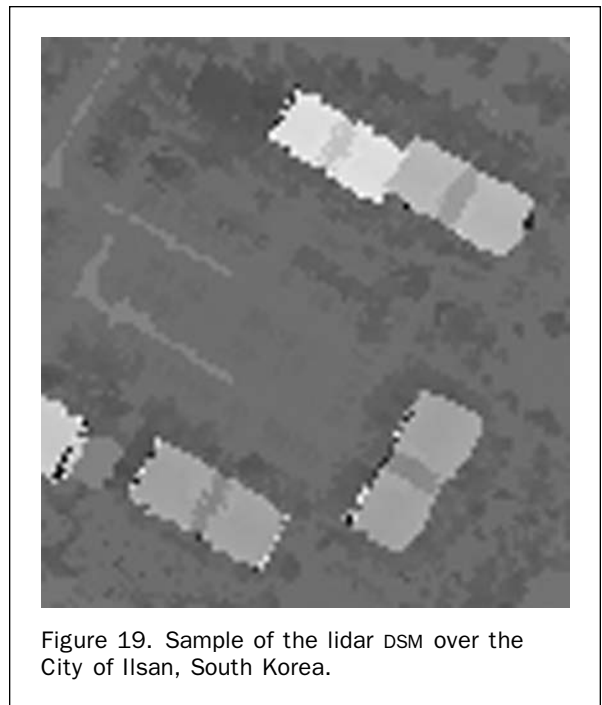
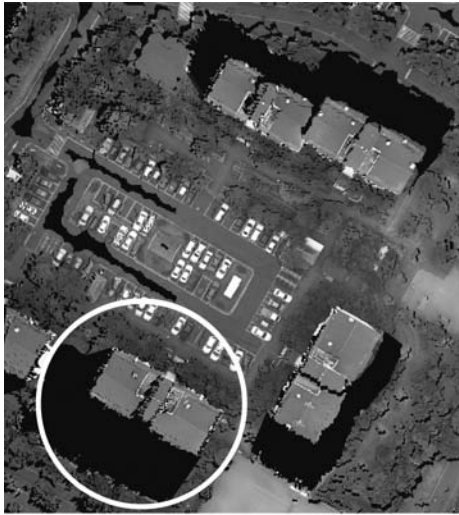


Figure 19. Sample of the lidar DSM over the City of Ilsan, South Korea.

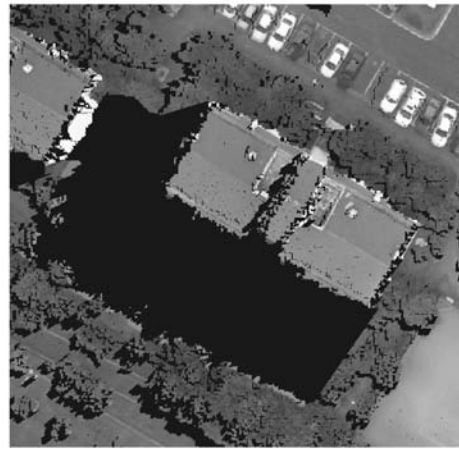
The execution time for generating the orthophotos using the adaptive radial sweep and Z-buffer methodologies turned out to be almost the same. On the other hand, the execution of the spiral sweep methodology consumed a fraction of that time. Finally, generated true orthophotos from the twenty-three images in this dataset are tiled together in Figure 23a. In that figure, occluded cells in each of the tiles are filled using those in overlapping orthophotos. Figure 23b is a closer look at a 3D perspective view resulting from draping the true orthophoto on top of the DSM. These figures indicate the good quality and the improved value of the final product.

Conclusions and Recommendations

The wide adoption of GIS databases has increased the demand for orthophotos. In the mean time, the improved resolutions and performance of current imaging, ranging, and georeferencing systems are allowing for the production of high quality orthophotos. Unfortunately, high-resolution imaging sensors are magnifying the relief displacement effects especially when mapping urban areas. For this imagery, true orthophoto generation techniques are essential to assure reliable interpretability and maintain the high quality of the available data. Therefore, there has been a significant interest within the photogrammetric community to develop true orthophoto generation methodologies. The most popular techniques for true orthophoto generation are based on the Z-buffer methodology. This methodology is sensitive to the relative relationship between the DSM cell size and the GSD of the imaging sensor. Incompatibility between the DSM and ground image resolutions will lead to false visibilities and occlusions. Moreover, the Z-buffer methodology requires the availability of a DBM, where artificial points along building facades are introduced. This paper introduced two new methodologies, adaptive radial sweep and spiral sweep, for occlusion detection and true orthophoto generation. Both methodologies are based on checking the off-nadir angle to the line of sight connecting the perspective center of the imaging sensor and the DSM cells. Both methodologies have no requirements with regard



(a)

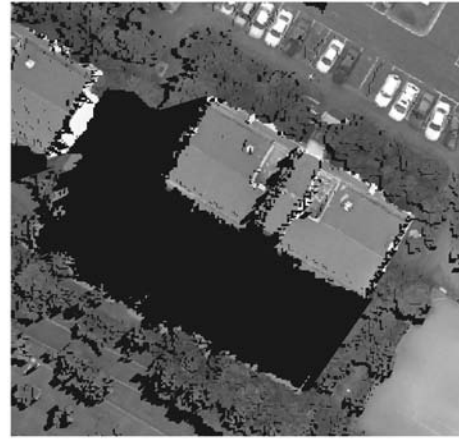


(b)

Figure 20. True orthophoto generated using the adaptive radial sweep (a) with a closer look at the building within the white circle (b).



(a)



(b)

Figure 21. True orthophoto generated using the spiral sweep (a) with a closer look at the building within the white circle (b).

to the sampling interval of the DSM as well as the availability of a DBM. Experimental results with simulated and real data have shown the improved performance of both methodologies when compared to the traditional Z-Buffer technique.

Future research will focus on utilizing detected occlusions to generate hypotheses about the existence of man-made structures. These hypotheses will be then refined to generate an accurate DBM. Finally, generated true orthophotos together with the DSM and DBM will be combined to produce realistic 3D perspective views of the mapped areas. For urban areas, these views can be augmented with terrestrial imagery to produce complete 3D city models. Future research will also focus on

adjusting the gray values in generated orthophoto mosaics to assure seamless transition between neighboring orthophotos.

Acknowledgments

The authors would like to thank Mr. Paul Mrstik, Terrapoint Canada, Inc. for providing the lidar and image datasets, which was utilized in the experimental results section. The authors are also indebted to Mr. Mrstik for the numerous valuable discussions of the research outcome. This research work has been conducted under the auspices of the GEOIDE Research Network through its financial support of the project (SII 43).



(a)



(b)

Figure 22. True orthophoto generated using the Z-buffer (a) with a closer look at the building within the white circle (b).



(a)



(b)

Figure 23. True orthophoto mosaic (a) with a 3D perspective view (b) of the portion enclosed by the white circle.

References

- Amhar, F., and R. Ecker, 1996. An integrated solution for the problems of 3D man-made objects in digital orthophotos, *International Archives of Photogrammetry and Remote Sensing*, 31(Part B4): 84–89.
- Amhar, F., J. Jansa, and C. Ries, 1998. The generation of true orthophotos using a 3D building model in conjunction with a conventional DTM, *International Archives of Photogrammetry and Remote Sensing*, 32(Part 4):16–22.
- Catmull, E., 1974. A Subdivision Algorithm for Computer Display of Curved Surfaces, Ph.D. dissertation, Department of Computer Science, University of Utah, Salt Lake City, Utah.
- Konecny, G., 1979. Methods and possibilities for digital differential rectification, *Photogrammetric Engineering & Remote Sensing*, 45(6):727–734.
- Kraus, K., 1993. *Photogrammetry*, Dümmler Verlag, Bonn, Volume 1, 397 p.
- Kuzmin, P., A. Korytnik, and O. Long, 2004. Polygon-based true orthophoto generation, *XXth ISPRS Congress Proceedings*, 12–23 July, Istanbul, pp. 529–531.
- Mikhail, E., 2001. *Introduction to Modern Photogrammetry*, John Wiley & Sons, Inc., New York, 479 p.
- Novak, K. 1992. Rectification of digital imagery, *Photogrammetric Engineering & Remote Sensing*, 58(3):339–344.
- Rau, J., N. Chen, and L. Chen, 2000. Hidden compensation and shadow enhancement for true orthophoto generation, *Proceedings of Asian Conference on Remote Sensing 2000*, 04–08 December, Taipei, unpaginated CD-ROM.
- Rau, J., N. Chen, and L. Chen, 2002. True orthophoto generation of built-up areas using multi-view images, *Photogrammetric Engineering & Remote Sensing*, 68(6):581–588.
- Sheng, Y., P. Gong, and G. Biging, 2003. True orthoimage production for forested areas from large-scale aerial photographs, *Photogrammetric Engineering & Remote Sensing*, 69(3):259–266.
- Skarlatos, D., 1999. Orthophotograph production in urban areas, *The Photogrammetric Record*, 16(94):643–650.
- Sutherland, I., R. Sproull, and R. Schumacker, 1974. A characterization of ten hidden-surface algorithms, *ACM Computing Surveys*, 6:1–55.
- Zhou, G., 2005. Urban Large-scale Orthoimages Standard for National Orthophoto Program, *XXVth IEEE International Geoscience and Remote Sensing Symposium Proceedings*, 25–29 July, Seoul, Korea, unpaginated CD-ROM.

(Received 05 July 2005; accepted 07 September 2005; revised 28 September 2005)